Revision 2
To be submitted to *American Mineralogist*
Prepared in October 2019; revision 1 in March 2020; revision 2 in March 2020

Vanadium micro-XANES determination of oxygen fugacity in olivine-hosted glass inclusion and groundmass glasses of martian primitive shergottite Yamato 980459

Ryoichi Nakada [a,b]*, Tomohiro Usui [b§], Masashi Ushioda [c], Yoshio Takahashi [d]

[a] Kochi Institute for Core Sample Research, Japan Agency for Marine-Earth Science and Technology (JAMSTEC), Monobe 200, Nankoku, Kochi 783-8502, Japan
[b] Earth-Life Science Institute, Tokyo Institute of Technology, Meguro, Tokyo 152-8550, Japan
[§]Present address: Institute of Space and Astronautical Science, Japan Aerospace Exploration Agency. 3-1-1 Yoshinodai, Sagamihara, Kanagawa 252-5210, Japan
[c] Geological Survey of Japan, National Institute of Advanced Industrial Science and Technology (AIST), Central 7, 1-1-1 Higashi, Tsukuba, Ibaraki 305-8567, Japan
[d] Department of Earth and Planetary Science, The University of Tokyo, Hongo 7-3-1, Bunkyo, Tokyo 113-0033, Japan

*Corresponding author
Tel.: +81-88-878-2275; fax: +81-88-878-2192.
E-mail address: nakadar@jamstec.go.jp (R. Nakada).

ABSTRACT

The redox condition of magma determines the stability and composition of crystallizing and volatile phases in martian meteorites, reflecting the evolution of the martian interior. In the current study, direct analyses on the oxidation states of V, Cr, and Fe were performed based on the X-ray absorption near-edge structure (XANES) measurements equipped with a micro-sized X-ray beam. We first applied the micro-XANES (μ-XANES) technique to the olivine-hosted glass inclusion and groundmass glass of martian meteorite Yamato 980459 (Y98), which is interpreted as representing a primary melt composition. Mass balance calculations and XANES spectra comparisons indicated that, while chromite and pyroxene affected Cr and Fe K-edge XANES spectra, the contribution of these minerals was minimal for V. The pre-edge peak intensity of V K-edge XANES enabled the estimation of the oxygen fugacity for inclusion and groundmass glasses. The calculated oxygen fugacity (fO_2) of the glass inclusions was near the Iron-Wüstite (IW) buffer (IW–0.07±0.32) for the glass inclusion, whereas it was 0.9 log units more oxidized (IW+0.93±0.56) for the groundmass glasses. This result suggests that the redox condition of the parent magma of Y98 evolved during magma ascent and emplacement. Since Y98 is interpreted to have evolved in a closed system, our finding suggests that fractional crystallization and/or ascent of magma potentially induces the fO_2 increase. This study shows that the μ-XANES technique enables us to determine the fO_2 by only measuring a single phase of glassy compounds, and thus, it is useful to discuss the redox condition of volcanic rocks even if they do not crystallize out several equilibrium phases of minerals.

Key words: μ-XANES; oxidation states, oxygen fugacity, Yamato 980459; shergottite

INTRODUCTION

The redox condition, or oxygen fugacity ($f\text{O}_2$), of magma controls the stability and composition of crystallizing and volatile phases in magma, and provides information on the genesis, differentiation, and source regions of the source mantle. Knowledge on the evolution of the martian interior is acquired by redox analysis of martian meteorite. The mineralogical oxybarometers, such as Fe-Ti oxides, have been conventionally applied to the estimation of $f\text{O}_2$ of martian magma (e.g., Stolper and McSween, 1979; Steele and Smith, 1982; McSween et al., 1996; Ghosal et al., 1998; Herd et al., 2001). The olivine-pyroxene-spinel oxybarometer has also been used for better estimation of the magmatic $f\text{O}_2$ (e.g., Herd et al., 2002; Goodrich et al., 2003; Herd, 2003; Peslier et al., 2010; Castle and Herd, 2017). Partitioning of redox-sensitive elements such as Eu (Wadhwa, 2001; Herd et al., 2002; McCanta et al., 2009) and transition metals including V, Cr, and Fe (Shearer et al., 2006; Karner et al., 2007a, 2007b, 2008; Papike et al., 2013) have been used to evaluate $f\text{O}_2$ more recently, in combination with laboratory experiments. Nowadays, in addition to these methods, the direct analysis of the oxidation states of an element of interest using X-ray absorption near edge structure (XANES) analysis has become an additional method for estimating the $f\text{O}_2$ of martian magma (Bell et al., 2014; Satake et al., 2014). These previous studies showed that $f\text{O}_2$ range of martian magma was mostly from –1 to +2 relative to Iron-Wüstite (IW) buffer, which is more reducing than Earth's basalts (IW+2 to IW+6), but slightly more oxidized than lunar basalts (IW–2 to IW±0) (Papike et al., 2004). When oxidized groundmasses are included, the $f\text{O}_2$ of martian basaltic lithology is up to IW+4 (Castle and Herd, 2017).

These previous studies, which estimated the $f\text{O}_2$ of martian magma based on several of the approaches described above, did not pay much attention to glassy compounds. For instance, olivine-hosted glass inclusion and groundmass glasses generally crystallize at the earliest and latest stages of the formation of basaltic rocks, respectively. This fact means that the investigation of these contrasting glass phases have the potential to provide information on the transition or evolution of the fO_2 from the initial basaltic magma generation to the final solidification stages. Analysis by XANES on the redox-sensitive elements could provide novel insights into the estimation of the fO_2 of glass in martian meteorite because XANES is applicable to glass.

The direct analysis of the oxidation state would be more valuable for glassy compounds than for minerals because chemical species in a mineral are not only controlled by the redox condition, but also by the crystal structure of the host mineral. A good example can be found in the Earth's lower mantle. The fO_2 of the Earth's lower mantle is lower than that of the upper mantle, even though the abundance of ferric Fe in the lower mantle is higher than that of the upper mantle (McCammon, 2005). This paradox is explained by the redox-independent substitution of Fe^{3+} with Al^{3+} in the aluminous silicate perovskite, which is the dominant mineral in the lower mantle (Frost et al., 2004). Typically, the oxidation state of an element in a mineral does not mirror the redox condition of its host rock. Consequently the most useful phases to estimate fO_2 of a martian magma using XANES is to analyze the inclusion and matrix glasses of a martian meteorite.

This study presents micro-XANES (μ-XANES) analysis of V, Cr, and Fe in both inclusion and groundmass glasses of a martian meteorite with the goal to estimate the fO_2 and evolution of martian magma. Results on Cr and Fe analyses are presented and discussed in the supplemental information. The determination of the oxidation states of V can offer reasonable clues toward the estimation of the $f\mathrm{O}_2$ of magma, taking into account the fact that (i) V is highly redox-sensitive, reflecting various oxidation states over a wide range of $f\mathrm{O}_2$ experienced by planetary basalts (Carmichael and Ghiorso, 1990; Papike et al., 2004, 2005), and (ii) the concentrations of V is high enough to yield accurate oxidation states based on XANES analysis. The martian meteorite examined in this study was Yamato 980459 (Y98), which is an olivine-phyric shergottite and represents a primary melt composition that evolved in a closed system (Greshake et al., 2004; Mikouchi et al., 2004; Usui et al., 2008). Accordingly, the application of micro-XANES to glass in the Y98 martian meteorite has significant potential for the direct determination of the log $f\mathrm{O}_2$ condition of V in the evolving melt before and during crystallization.

SAMPLES AND METHODS

Yamato 980459

Petrological and geochemical studies showed that Y98 represents a primary melt composition (Greshake et al., 2004; Mikouchi et al., 2004; Usui et al., 2008). The olivine-phyric shergottite Y98 is composed of magnesian olivine megacrysts, pyroxene, chromite, and glassy mesostasis filled mainly with dendritic olivine and augite (Greshake et al., 2004; Usui et al., 2008), whereas characteristics related to the impact glasses were not observed. Glassy melt inclusions, which are mostly enclosed within olivine, were observed. The inclusions are believed to record the progressive collection of melt components from a residual olivine, pyroxene, and garnet mantle source (Peters et al., 2015). Both groundmass and melt inclusions were interpreted as having been formed by rapid cooling during eruption with a cooling rate of 1000°C/h, which is suggested by the quenched textures (Greshake et al., 2004). Usui et al. (2012) showed that volatile elements may be degassed from the inclusions, but major elements represented a magmatic trend in the closed system. Geochemical data show that Y98 is a depleted shergottite crystallized at 472 Ma (Shih et al., 2005). Partitioning of V between olivine and liquid shows that the fO_2 of Y98 primary magma was approximately IW+1 (Shearer et al., 2006), which is also supported by the Cr valence analysis in olivine (Bell et al., 2014).

Micro-XANES measurements

Synthesized silicate glasses. In this study, a Y98 glass was synthesized to calibrate fO_2 based on V XANES. The major element compositions were analogous to the Y98 inclusion glass (Usui et al., 2008) but doped with V. Approximately 10 g of a well-mixed powder of reagents (SiO_2, TiO_2, Al_2O_3, FeO, MnO, MgO, $CaCO_3$, Na_2CO_3, K_2CO_3, P_2O_5, and V_2O_3) was placed in a platinum crucible and heated from room temperature to 600ºC in 1 h using a muffle furnace. The sample's temperature was raised to 900ºC in 3 h and kept at that temperature for 10 h. The sample was then placed in a SiC furnace heated at 1450ºC for 3 h, and quenched to room temperature. During the use of the furnace, oxygen fugacity was controlled by mixing of H_2 and CO_2 gases using gas flowmeters to obtain IW±0, +0.7, and +2.2. A terrestrial basaltic glass, with a normal mid-ocean ridge basalt (N-MORB) composition [synthesized at Quartz-Fayalite-Magnetite (QFM) buffer (IW+3.4; Nakada et al., 2017) condition], was also measured for comparison.

Vanadium K-edge XANES. A polished thin section of Y98 (#51-2) (Fig. 1) was used in this study. The V K-edge (5465 eV) μ-XANES analyses were performed using the undulator beamline BL05XU at the SPring-8, Hyogo, Japan. The white beam from an undulator was monochromatized using a Si(111) double-crystal monochromator. The X-ray beam was focused using a K-B mirror to a final spot size of 1.2 (vertical) μm × 1.5 (horizontal) μm. The measurements were conducted at ambient pressure and temperature. The spectra of reference materials, such as metal foil, V_2O_3, VO_2, and V_2O_5 reagents (Wako Pure Chem. Ind., Ltd., Osaka, Japan) were measured in transmission mode, whereas those of the Y98 sample and synthesized silicate glasses were acquired in fluorescence mode. In the latter mode, X-ray fluorescence (XRF) signals of the sample placed at 45° to the incident beam were obtained using a single element silicon drift detector (SDD) positioned 90° to the incident beam. Prior to the μ-XANES measurements, XRF mapping that was scanned in 5 μm steps was obtained to determine the analytical spot with reference to the backscattered electron images (Usui et al., 2008). The X-ray energy was calibrated by defining the first peak in the first derivative spectrum of V foil as 5465 eV, which is the same energy as in the previous studies (Sutton et al., 2005). Repeated XANES scans of Y98 analytical spots yielded indistinguishable change among them, showing that any X-ray-induced alteration of the samples was unlikely in our measurements.

In this study, the Cr and Fe K-edge XANES were also measured. However, contribution of Cr and Fe fluorescent X-rays from minerals were identified for Y98 glass (see Discussion section), and thus, Cr and Fe measurements are described in the Supplementary Information.

Analyses on the redox condition of Y98

The V K-edge XANES spectra were analyzed following the procedure reported by

Sutton et al. (2005). The spectra were normalized at 5600 eV after background subtraction. The edge step contribution was subtracted from the pre-edge region around 5470 eV using a spline function. The maximum intensity in this net pre-edge region was multiplied by 1000. A calibration curve was obtained for the log fO_2 calculation by plotting the relationship between pre-edge peak intensity and log fO_2 relative to IW buffer of the three synthesized silicate glasses (Fig. 2). The observed pre-edge intensities of Y98 samples were input into the regression function to calculate the log fO_2.

RESULTS

XRF mapping

The back-scattered electron (BSE) image along with the tricolored XRF maps composed of Fe (red), Cr (green), and Ca (blue) around megacryst olivines are shown in Figs. 3A–3C, respectively. A glass inclusion and a groundmass glass are identified in and near an olivine, which are named Inc 1 and GM 1, respectively (Figs. 3D and 3E). Another inclusion and groundmass glass identified in and near an olivine are named as Inc 2 and GM 2 (Figs. 3F and 3G). A groundmass around a pyroxene below another megacryst olivine is further examined (named GM 3; Fig. 3H). A groundmass around another megacryst olivine, hereafter named GM 4, is also measured for μ-XANES (Fig. 3I). As a whole, two olivine-hosted inclusion glasses and four areas of groundmass glass are selected for this study.

The XRF maps of each individual element, namely Fe, Cr, and Ca, are provided in the Supplementary Figures. A variation in the XRF intensity of Fe is observed in the measured area. The fluorescence X-ray signal is strongest for olivine, and those of pyroxene and groundmass are almost similar or slightly stronger than that in pyroxene [(A) of Supplementary Figs. 1–9]. This trend is consistent with the microprobe analysis performed in a previous study (Usui et al., 2008). In contrast to Fe, the Ca signal is weakened in the following order: glass, pyroxene, and olivine [(C) of Supplementary Figs. 1–9], which is also consistent with the electron microprobe analysis (Usui et al., 2008). The location where the strong Cr signal is observed is scattered, while Cr signals of the other areas are too small to recognize systematic signal changes [(B) of Supplementary Figs. 1–9]. The presence of chromite with Cr concentrations of ~60wt% as Cr_2O_3 accounts for the strong Cr signal. As a result, tricolor maps composed of Fe (red), Cr (green), and Ca (blue) show clear distinction among the minerals, such as bright red for Ol, dark red for pyroxene, purple to blue for glass, and green for chromite (Fig. 3).

Micro-XANES measurements

The V K-edge XANES spectra of reference materials clearly shows an increase in the pre-edge peak intensity with increasing valence state of V or redox condition (Fig. 4). Both oxide reagents and synthesized glass also show that the XANES oscillation in the spectrum weakens with increasing redox condition. For example, V_2O_3 reagent shows two-humped peaks at around 5485 eV and 5500 eV, whereas these peaks become smaller with higher oxidation states. Similarly, a magnitude of absorption maximum of synthesized glass at around 5483 eV decreases with increasing fO_2. The V K-edge XANES spectra of Y98 glasses shows a feature similar to those of the synthesized glasses: absorption maximum occurs at around 5483 eV with a shoulder at around 5494 eV (Fig. 4). Pre-edge maximum intensities of V in synthesized silicate glasses increases from 100 to

349 along with an increase in the fO_2 from IW±0 to +2.2 (Table 1). The pre-edge maximum intensities of V in inclusion and groundmass glasses vary from 86 to 125 and 178 to 257, resulting in the calculated log fO_2 range of –0.23 to +0.12 and +0.58 to +1.27 for inclusion and groundmass glasses, respectively (Table 1; Fig. 5). The mean log fO_2 range relative to IW of inclusion and groundmass glasses are –0.07±0.32 and +0.93±0.56, respectively. The Cr and Fe K-edge XANES data are described in the Supplementary Information.

DISCUSSION

Effect of minerals on the XANES spectra

The contributions of Cr- and Fe-bearing minerals (chromite, Cr-spinel, and pyroxene) to the analyzed glass were observed by Cr and Fe XANES (Supplementary Figs. 11 and 12). The influence of chromite grains on the Cr K-edge μ-XANES spectra of spot 1 in Inc 2 and spot 1 in GM 3 can be considered because chromite grains were identified near the analyzed spots (Figs. 3C and 3D). Irradiation on the chromite grains would affect the XANES spectra of Y98 as shown by the measured spectra, particularly the third absorption peak at around 6062 eV (Supplementary Fig. 11).

In a similar way to the Cr-XANES features, the contributions of olivine and augite dendrites may not be negligible in the Fe K-edge XANES spectra because the groundmass glass is filled with these fine dendritic crystals (Greshake et al., 2004; Usui et al., 2008). The characteristics of pyroxene represented by two-humped peaks or olivine showing a sharp peak around 7123 eV with a small shoulder 7136 eV were observed in the XANES spectra obtained in GM 2–4 (Supplementary Figs. 12). Although irradiation of these dendrites affected the XANES spectra to some degree, pre-edge analysis of groundmass glass showed that mean Fe oxidation states were higher than that in pyroxene or olivine (Table 1). This fact suggests that the irradiation of Fe-bearing dendrites does not significantly disturb the oxidation state analysis of Fe.

While the Cr and Fe XANES spectra could be irregularly disturbed by Cr- and Fe-bearing minerals, the influence of these minerals that contain V to some degree on the V XANES spectra is found to be less significant. The V K-edge XANES spectra of Y98 glasses does not exhibit intense white lines and presents a similar feature with those of synthesized glasses (Figs. 4B and 4C). Among the constituent minerals in Y98, V is mostly partitioned to chromite with abundances up to 0.41 wt% as V_2O_3 (Usui et al., 2008), which is approximately two orders of magnitude higher than those of olivine or orthopyroxene (33.6 and 90 ppm, respectively; Usui et al., 2008). Hence, the following discussion focuses on the contribution of chromite to the V XANES spectrum. A partitioning experiment showed that the partition coefficient of V between olivine and melt ($D^{\mathrm{olivine/melt}}_{\mathrm{V}}$, defined by measured $\mathrm{V}_{\mathrm{olivine}}$/measured $\mathrm{V}_{\mathrm{melt}}$) was 0.30 and 0.18 at IW and IW+1, respectively (Shearer et al., 2006), meaning that V contents in glass are calculated to be 112–187 ppm. This value is presumably close to the V contents in the measured olivine-hosted glass inclusions because olivine was the first liquidus phase of Y98 parent melt (Musselwhite et al. 2006). Similarly, the $D^{\mathrm{orthopyroxene/melt}}_{\mathrm{V}}$ was 0.97 and 0.82 at IW and IW+1, respectively (Papike et al., 2014), which enables us to estimate the V contents in groundmass glass as being 93–110 ppm. Thus, the V concentration in the glass is approximately 1/40 lower than that of chromite.

Here, we have examined the effect of chromite irradiation on the V valence by calculating the V valence of “original” glasses without artifact from the presence of chromite in the glass. As for the most conservative (i.e., worst) case, V contents were assumed to be 112 and 93 ppm (i.e., lowest) for inclusion and groundmass glasses, respectively, whereas that of chromite was 4100 ppm. In our measurement, the V pre-edge intensity of chromite was 96.8, and thus the calculated fO_2 of chromite was IW–0.13. In the case of spot 1 of Inc 1, the measured fO_2 was IW+0.12 (Table 1). If the content of chromite containing 4100 ppm of V with a valence of IW–0.13 is 10% in the glass which affected the observed signal, the V contents and fO_2 of the “original” (or unirradiated) inclusion glass should be 100.8 ppm and IW+1.14, respectively (Fig. 6). If the fraction of chromite in the irradiated part of the glass was 1%, the measured result is explained by the mixture of chromite containing 41 ppm of V crystallized at IW–0.13 with an “original” glass component with 110.9 ppm of V crystallized at IW+0.21. These calculations suggest that the irradiation of chromite may have significantly affected the V signal from inclusion glass and resulted in the underestimation of the measured V valence. If the contribution of V from chromite in the irradiated part was 0.01%, the V contents and fO_2 of inclusion glass free from the contribution of chromite were calculated to be 112 ppm and IW+0.12, respectively. These values do not affect the measured result. Similarly, the calculation was conducted for other measured locations on inclusion and groundmass glass to estimate the contribution from chromite irradiation. In all cases, our calculations showed that irradiation that is less than 0.1% chromite grain does not affect the estimated fO_2 based on V K-edge XANES spectra, when V contents are 112 and 93 ppm for inclusion and groundmass glass, respectively, which are the most conservative V contents (Fig. 6). The contribution of chromite can be smaller than 0.1% because (i) the X-ray beam size was

1.2 (vertical) μm × 1.5 (horizontal) μm for the V measurement, which is small enough to avoid irradiating the chromite grain and (ii) the XRF signal of Cr does not show a gradual change and its intensities of analytical spots are similar to other glasses located far from chromite grains which must not affect the Cr signal of the glass ((B) of Supplementary Figs. 1–9). Indeed, the Cr concentration in the inclusion and groundmass glasses varies from 0.1 to 0.3 wt% and 0.01 to 0.2 wt%, respectively, which is about three orders of magnitude lower than that of chromite (~60 wt%; Usui et al., 2008; 2012). The mass balance analysis suggests that irradiation of about 0.0017 to 0.005% and 0.00017 to 0.0033% of chromite grain within an analytical spot compensates for the Cr signal to inclusion and groundmass glass, respectively. These data indicate that the V XANES spectra are not affected by the irradiation of minerals. Thus, we discuss the $f\mathrm{O}_2$ based on the V measurement.

The $f\mathrm{O}_2$ estimation based on the pre-edge peak intensity of V

The average oxidation state of Fe was not used to estimate $f\mathrm{O}_2$ because (i) Fe XANES spectra suggest contribution from pyroxene or chromite, and (ii) a calibration curve for the estimation of $f\mathrm{O}_2$ based on the oxidation state of Fe is not valid when Fe(II) is dominant (Kress and Carmichael, 1991). Instead, the pre-edge peak intensity of V reflects oxygen fugacity, although it can be affected by the crystallization temperature and melt composition (Sutton et al., 2005). In the current study, the calibration curve was obtained using synthesized glasses whose compositions mimic Y98 quenched from 1450°C, which is the 1 bar liquidus temperature of Y98 determined by an experiment (Koizumi et al., 2004). The glass inclusions were trapped as melt in olivine megacryst cores with ~Fo_{80} (Usui et al., 2012). Equilibrium experiments on a synthetic Y98 composition showed that Fo_{80} olivine crystallized at around 1470°C (Rapp et al., 2013), which is comparable to the 1 bar liquidus temperature of Y98 (1450°C; Koizumi et al., 2004) and of our synthesized glass standards. Both inclusion and groundmass glasses experienced the same rapid cooling during the eruption (1000°C/h; Greshake et al., 2004), suggesting that the behavior of V in groundmass glass should be the same to that of the inclusion glass during decreasing liquid temperature. Although the previous study showed that the Ti content affects the pre-edge peak intensity of V (Sutton et al., 2005), the similar Ti contents in inclusion and groundmass glasses (1.00 and 0.99–1.08wt.% as TiO_2, respectively (Usui et al., 2012)) do not affect the pre-edge peak intensity of V in the current study. The relationship between the pre-edge peak intensity and oxygen fugacity of synthetic glasses used in this study is shown in Fig. 2. The linear regression showed a good correlation ($r^2 = 0.98$) and was used as a calibration curve for the analyzed V intensity of Y98.

Compared to previous studies estimating the fO_2 of the Y98 parent magma (Shearer et al., 2006; Bell et al., 2014), the current study suggests an almost identical or slightly more reduced redox conditions for the mantle source. The oxygen fugacity during the spinel crystallization of Y98 was estimated to be IW+0.9 (McKay et al., 2004). The partitioning of V between olivine and melt also suggested that the fO_2 of Y98 was IW+0.9 (Shearer et al., 2006). Trace element systematics (Mn–Ni–Co–Cr–V) of olivine megacrysts suggested that the megacrysts crystallized at ~IW+1 condition (Usui et al., 2008). The partitioning of V and Cr between pyroxene and melt resulted in IW±0 to IW+1 (Karner et al., 2007a), although V partitioning with pyroxene can be controlled by the composition and crystal structure of the pyroxene (Papike et al., 2014). The current study uses μ-XANES analyses of inclusion and groundmass glasses, which gave consistent results on the fO_2 of the Y98 parent magma with these previous studies. Thus, our new approach, μ-XANES local analysis on glassy compounds, is useful to estimate the redox condition of a magma; in particular, we successfully captured the initial fO_2 at the time of crystallization.

The μ-XANES analysis clearly showed different redox conditions between inclusion and groundmass glass, representing the earliest and the latest stages of magma crystallization. Hence, it is not surprising that groundmass glass showed a more oxidizing condition than the inclusion glass. The fO_2 increase during magma evolution is also reported for lithology A of Elephant Moraine (EET-A) 79001, North West Africa (NWA) 1068/1110, Larkman Nunatak (LAR) 06319, and Tissint (Goodrich et al., 2003; Herd, 2006; Peslier et al., 2010; Castle and Herd, 2017) (Fig. 7) based on mineralogical oxybarometers. Shergottites are characterized by the wide variation of incompatible elements classified by $^{87}Sr/^{86}Sr$ or $\varepsilon^{143}Nd$ values, and the fO_2 is increased as the reservoir enriched in incompatible elements (Wadhwa, 2001; Herd et al., 2002). Comparisons between the earlier and later crystallized phases shows that the fO_2 of enriched and depleted shergottites increased approximately two log units, whereas that of intermediate shergottites increased about one log unit during crystallization.

Although the mineralogical oxybarometer is a reliable method to estimate fO_2, it requires at least a pair of phases that are chemically in equilibrium with each other. In this respect, the best merit on performing the XANES analysis is that it can be applied to a single phase of glassy compounds. This fact means that, as shown in this study, the redox condition of volcanic rocks is more easily determined even if they do not crystallize out several kinds of minerals. This is the prime reason why the current study showed an fO_2 increase of Y98 that has strong chemical zoning of olivine and pyroxene reflecting the crystallization under a disequilibrium condition with kinetic effect (Greshake et al., 2004; Mikouchi et al., 2004; Usui et al., 2008). It should be noted that this study showed the second example of the fO_2 increase during magma crystallization of a geochemically depleted shergottite. The other study showed the fO_2 increase in the Tissint meteorite using a mineralogical oxybarometer (Castle and Heard, 2017). On the other hand, μ-XANES analysis directly indicated different redox conditions between the earliest and the latest stage of magma crystallization.

IMPLICATIONS FOR REDOX EVOLUTION DURING MAGMA ASCENT

Several models have been proposed to explain the fO_2 evolution during a single magmatic event: (i) assimilation of oxidized crustal material (Herd et al., 2002), (ii) magmatic fractional crystallization and ascent (Peslier et al., 2010) including auto-oxidation (Shearer et al., 2013; Castle and Herd, 2017). In the case of Y98, the most important constraint to consider the fO_2 evolution during magma crystallization is the fact that Y98 evolved in a closed system (Greshake et al., 2004; Usui et al., 2008). Therefore, model (i) is not responsible for increasing the fO_2 of the Y98 parent magma during its crystallization. Instead, candidate (ii) would cause the fO_2 increase. A possible chemical reaction to increase the fO_2 is the crystallization of olivine and pyroxene that selectively consumes divalent Fe, resulting in the increase of trivalent Fe in the remaining melt phase. This phenomenon is also shown in our XANES measurement (Fig. 5). Another chemical reaction is the degassing of volatiles, which has already been suggested for terrestrial magmas (Burgisser and Scaillet, 2007). While Usui et al. (2008) indicated that Y98 magma evolved in a closed system in terms of litho- and siderophile elements, the depletion of H due to magmatic degassing was suggested by the measurements of volatile elements in inclusion and groundmass glasses of Y98 (Usui et al., 2012).

In the case of Earth, the oxidation state of Fe in melt inclusion is indistinguishable from that in groundmass of mid ocean ridge basalt (MORB) (Kelley and Cottrell, 2009; Brounce et al., 2014). This fact means that, in contrast to Y98, the redox evolution during the magmatic fractional crystallization and ascent does not occur in the MORB system. The fO_2 of the Earth's mantle is higher than that of the martian mantle because oxidized materials are introduced into the upper mantle through the subduction of surface materials and self-oxidation of the lower mantle via crystallization of magnesium silicate perovskite (Frost et al., 2004; Wood et al., 2006). The lack of these mechanisms on Mars might have kept the martian mantle reducing, and thus, the greater fO_2 gap between the reduced mantle and the oxidizing surface would have induced the fO_2 increase during the magmatic fractional crystallization and ascent process of the Y98 parent magma. A preferential partitioning of reduced V into minerals during the crystallization results in the enrichment of oxidized V in the groundmass glass. The auto-oxidation with degassing causes a dramatic fO_2 increase. The crystallization history of NWA1183 from olivine core to rim experienced the a fO_2 increase from ~IW+1.8 to QFM+0.5 (Shearer et al., 2013). Similarly, an approximately 2.1 log unit increase of fO_2 is suggested during the crystallization of the Tissint magma, caused by the auto-oxidation and degassing (Castle and Herd, 2017). In contrast to these studies, our measurement only showed approximately a one log unit increase of in fO_2, which can only be explained only by auto-oxidation as suggested by MELTS thermodynamic models (Castle and Herd, 2017).

Although the cause of the fO_2 increase in melt of Y98 melt is still debatable, the current study demonstrated that the μ-XANES measurement of glass compounds can serve as an alternative method to examine the fO_2 increase of a martian meteorite, and also confirmed that fO_2 increase during magma fractionation is a common phenomenon on Mars.

ACKNOWLEDGMENTS

Scientific discussion with members of the Mars Science Team of Tokyo Tech was fruitful and improved the study. The authors are grateful to Dr. Anne Peslier, AE of this manuscript, and Drs. Aaron Bell and Steve Sutton for providing suggestions and comments that helped improve the manuscript. The authors applicate Dr. Lucy Kwok for English editing. This work was partly supported by Kurita Water and Environment Foundation (14E044) and JSPS KAKENHI Grant Numbers (15K17793, 15KK0153, 16H04073, and 17H06458). The speciation of V, Cr, and Fe were measured with the approval of SPring-8 (2017B1060, 2017B1854, 2018A1108, and 2018A1759), ALS (Proposal No. ALS-06699), and KEK-PF (Proposal No. 2015G137, 2016G114, and 2017G116), respectively. ALS is an Office of Science user facility supported by the DOE under contract No. DE-AC02-05CH11231.

REFERENCES

Bell, A.S., Burger, P.V., Le, L., Shearer, C.K., Papike, J.J., Sutton, S.R., Newville, M., and Jones, J. (2014) XANES measurements of Cr valence in olivine and their applications to planetary basalts. American Mineralogist 99, 1404–1412.

Berry, A.J., and O'Neill, H.St.C. (2004) A XANES determination of the oxidation state of chromium in silicate glasses. American Mineralogist 89, 790–798.

Brounce, M.N., Kelley, K.A., and Cottrell, E. (2014) Variations in $Fe^{3+}/\Sigma Fe$ of Mariana arc basalts and mantle wedge fO_2. Journal of Petrology 55, 2513–2536.

Burgisser, A., and Scaillet, B. (2007) Redox evolution of a degassing magma rising to the surface. Nature 445, 194–197.

Carmichael, I.S.E., and Ghiorso, M.S. (1990) The effect of oxygen fugacity on the redox states of natural liquids and their crystallizing phases. In J. Nicholls, and J.K. Russell, Eds., Modern methods of igneous petrology: understanding magmatic processes, vol. 24, Mineralogical Society of America, Washington, pp. 190–212.

Castle, N., and Herd, C.D.K. (2017) Experimental petrology of the Tissint meteorite: Redox estimates, crystallization curves, and evaluation of petrogenetic models. Meteoritics & Planetary Science 52, 125–146.

Chou, I.C. (1987) Oxygen buffer hydrogen sensor techniques at elevated pressures and temperatures. In G.C. Ulmer, and H.L. Barnes, Eds., Hydrothermal Experimental Techniques, pp. 61–99. New York, Wiley.

Frost, D.J., Liebske, C., Langenhorst, F., McCammon, C.A., Trønnes, R.G., and Bubie, D.C. (2004) Experimental evidence for the existence of iron-rich metal in the Earth's lower mantle. Nature 428, 409–412.

Ghosal, S., Sack, R.O., Ghiorso, M.S., and Lipschutz, M.E. (1998) Evidence for a reduced, Fe-depleted martian mantle source region of shergottites. Contributions to Mineralogy and Petrology 130, 346–357.

Giuli, G., Pratesi, G., Cipriani, C., and Paris, E. (2002) Iron local structure in tektites and impact glasses by extended X-ray absorption fine structure and high-resolution X-ray absorption near-edge structure spectroscopy. Geochimica et Cosmochimica Acta 66, 4347–4353.

Goodrich, C.A., Herd, C.D.K., and Taylor, L.A. (2003) Spinels and oxygen fugacity in olivine-phyric and lherzolitic shergottites. Meteoritics & Planetary Science 38, 1773–1792.

Greshake, A., Fritz, J., and Stoffler, D. (2004) Petrology and shock metamorphism of the olivine-phyric shergottite Yamato 980459: evidence for a two-stage cooling and a single-stage ejection history. Geochimica et Cosmochimica Acta 68, 2359–2377.

Herd, C.D.K., Papike, J.J., and Brearley, A.J. (2001) Oxygen fugacity of martian basalts from electron microprobe oxygen and TEM-EELS analyses of Fe-Ti oxides. American Mineralogist 86, 1015–1024.

Herd, C.D.K., Borg, L., Jones, J.H., and Papike, J.J. (2002) Oxygen fugacity and geochemical variations in martian basalts: Implications for martian basalt petrogenesis and the oxidation of the upper mantle of Mars. Geochimica et Cosmochimica Acta 66, 2025–2036.

Herd, C.D.K. (2006) Insights into the redox history of the NWA 1068/1110 martian basalt from mineral equilibria and vanadium oxybarometry. American Mineralogist 91, 1616–1627.

Jones, J.H. (2015) Various aspects of the petrogenesis of the Martian shergottite meteorites. Meteoritics & Planetary Science 50, 1–17.

Karner, J.M., Papike, J.J., Shearer, C.K., McKay, G., Le, L., and Burger, P. (2007a) Valence state partitioning between pyroxene-melt: Estimates of oxygen fugacity for martian basalt QUE 94201. American Mineralogist 92, 1238–1241.

Karner, J.M., Papike, J.J., Sutton, S.R., Shearer, C.K., McKay, G., Le, L., and Burger, P. (2007b) Valence state partitioning of Cr between pyroxene-melt: Effects of pyroxene and melt composition and direct determination of Cr valence states by XANES. American Mineralogist 92, 2002–2005.

Karner, J.M., Papike, J.J., Sutton, S.R., Shearer, C.K., Burger, P., McKay, G., and Le, L. (2008) Valence state partitioning of V between pyroxene-melt: Effects of pyroxene and melt composition, and direct determination of V valence states by XANES. Meteoritics & Planetary Science 43, 1275–1285.

Kelley, K.A., and Cottrell, E. (2009) Water and the oxidation state of subduction zone magmas. Science 325. 605–607.

Koizumi, E., Mikouchi, T., McKay, G., Monkawa, A., Chokai, J., and Miyamoto, M. (2004) Yamato980459: crystallization of Martian magnesian magma. Lunar and Planetary Science XXXV, Lunar Planet. Inst., Houston #1494.

McCammon, C. (2005) The paradox of mantle redox. Science 308, 807–808.

McCanta, M.C., Elkins-Tanton, L., and Rutherford, M.J. (2009) Expanding the application of the Eu-oxybarometer to the lherzolitic shergottites and nakhlites: implications for the oxidation state heterogeneity of the Martian interior. Meteoritics & Planetary Science 44, 725–745.

McSween, Jr.H.Y., Eisenhour, D.D., Taylor, L.A., Wadhwa, M., and Crozaz, G. (1996) QUE94201 shergottite: crystallization of a martian basaltic magma. Geochimica et Cosmochimica Acta 22, 4563–4569.

Mikouchi, T., Koizumi, E., McKay, G., Monkawa, A., Ueda, Y., Chokai, J., and Miyamoto, M. (2004) Yamato 980459: Mineralogy and petrolofy of a new shergottite-related rock from Antarctica. Antarctic meteorite research 17, 13–34.

Musselwhite, D.S., Dalton, H.A., Kiefer, W.S., and Treiman, A.H. (2006) Experimental petrology of the basaltic shergottite Yamato-980456: implications for the thermal structure of the Martian mantle. Meteoritics & Planetary Science 41, 1271–1290.

Nakada, R., Ogawa, K., Suzuki, N., Takahashi, S., and Takahashi, Y. (2014) Late Triassic compositional changes of aeolian dusts in the pelagic Panthalassa: response to the continental climatic change. Palaeogeography, Palaeoclimatology, Palaeoecology 393, 61–75.

Nakada, R., Shibuya, T., Suzuki, K., and Takahashi, Y. (2017) Europium anomaly variation under low-temperature water-rock interaction: A new thermometer. Geochemistry International 55, 822–832.

Papike, J.J., Karner, J.M., and Shearer, C.K (2004) Comparative planetary mineralogy: V/(Cr + Al) systematics in chromite as an indicator of relative oxygen fugacity. American Mineralogist 89, 1557–1560.

Papike, J.J., Karner, J.M., and Shearer, C.K. (2005) Comparative planetary mineralogy: Valence state partitioning of Cr, Fe, Ti, and V among crystallographic sites in olivine, and spinel from planetary basalts. American Mineralogist 90, 277–290.

Papike, J.J., Burger, P.V., Bell, A.S., Le, L., Shearer, C.K., Sutton, S.R., Jones, J., and

Newville, M. (2013) Developing vanadium valence state oxybarometers (spinel-melt, olivine-melt, spinel-olivine) and V/(Cr + Al) partitioning (spinel-melt) for martian olivine-phyric basalts. American Mineralogist 98, 2193–2196.

Papike, J.J., Burger, P.V., Bell, A.S., Shearer, C.K., Le, L., Jones, J., and Provencio, P. (2014) Valence state partitioning of V between pyroxene and melt for martian melt compositions Y 980459 and QUE 94201: The effect of pyroxene composition and crystal structure. American Mineralogist 99, 1175–1178.

Peslier, A.H. Hnatyshin, D., Herd, C.D.K., Walton, E.L., Brandon, A.D., Lapen, T.J., and Shafer, J.T. (2010) Crystallization, melt inclusion, and redox history of a Martian meteorite: Olivine-phyric shergottite Larkman Nunatak 06319. Geochimica et Cosmochimica Acta 74, 4543–4576.

Peters, T.J., Simon, J.I., Jones, J.H., Usui, T., Moriwaki, R., Economos, R.C., Schmitt, A.K., and McKeegan, K.D. (2015) Tracking the source of the enriched martian meteorites in olivine-hosted melt inclusions of two depleted shergottites, Yamato 980459 and Tissint. Earth and Planetary Science Letters 418. 91–102.

Rapp, J.F., Draper, D.S., and Mercer, C.M. (2013) Anhydrous liquid line of descent of Yamato-980459 and evolution of Martian parental magmas. Meteoritics & Planetary Science 48, 1780–1799.

Satake, W., Mikouchi, T., and Miyamoto, M. (2014) Redox states of thirteen shergottites as inferred from iron micro X-ray absorption near edge structure of maskelynite. Geochemical Journal 48, 85–98.

Shearer, C.K., McKay, G., Papike, J.J., and Karner, J.M. (2006) Valence state partitioning of vanadium between olivine-liquid: Estimates of oxygen fugacity of Y980459 and application to other olivine-phyric martian basalts. American Mineralogist 91, 1657–1663.

Shearer, C.K., Aaron, P.M., Burger, P.V., Guan, Y., Bell, A.S., and Papike, J.J. (2013) Petrogenetic linkages among fO_2, isotopic enrichments-depletions and crystallization history in Martian basalts. Evidence from the distribution of phosphorus in olivine megacrysts. Geochimica et Cosmochimica Acta 120, 17–38.

Shih, C.-Y., Nyquist, L.E., Wiesmann, H., Reese, Y., and Misawa, K. (2005) Rb–Sr and Sm–Nd dating of olivine-phyric Shergottite Y980459: petrogenesis of depleted Sher-gottites. Antarctic meteorite research 18, 46–65.

Shirai, N., and Ebihara, M. (2004) Chemical characteristics of a Martian meteorite, Yamato 980459. Antarctic meteorite research 17, 55–67.

Steele, I.M., and Smith, J.V. (1982) Petrography and mineralogy of two basalts and olivine-pyroxene-spinel fragments in achondrite EETA79001. Journal of Geophysical Research 87, A375–A384.

Stolper, E., and McSween, Jr.H.Y. (1979) Petrology and origin of the shergottite meteorites. Geochimica et Cosmochimica Acta 43, 1475–1498.

Sutton, S.R., Jones, K.W., Gordon, B., Rivers, M.L., and Smith, J.V. (1993) Reduced chromium in olivine grains from lunar basalt 15555: X-ray absorption near edge structure (XANES). Geochimica et Cosmochimica Acta 57, 461–468.

Sutton, S.R., Karner, J.M., Papike, J.J., Delaney, J.S., Shearer, C.K., Newville, M., Eng, P., Rivers, M.L., and Dyar, M.D. (2005) Vanadium K-edge XANES of synthetic and natural basaltic glasses and application to microscale oxygen barometry. Geochimica et Cosmochimica Acta 69, 2333–2348.

Usui, T., McSween, Jr.H.Y., and Floss, C. (2008) Petrogenesis of olivine-phyric sher-gottite Yamato 980459, revisited. Geochimica et Cosmochimica Acta 72, 1711–1730.

Usui, T., Alexander, C.M.O.D., Wang, J., Simon, J.I., Jones, J.H. (2012) Origin of water and mantle–crust interactions on Mars inferred from hydrogen isotopes and volatile element abundances of olivine-hosted melt inclusions of primi-tive shergottites. Earth and Planetary Science Letters 357, 119–129

Wadhwa, M. (2001) Redox state of Mars upper mantle and crust from Eu anomalies in shergottite pyroxenes. Science 291, 1527–1530.

Wilke, M., Farges, F., Petit, P.E., Brown, G.E., and Martin, F. (2001) Oxidation state and coordination of Fe in minerals: An Fe K-XANES spectroscopic study. American Mineralogist 86, 714–730.

Wilke, M., Farges, F., Partzsch, G.M., Schmidt, C., and Behrens, H. (2007) Speciation of Fe in silicate glasses and melts by in-situ XANES spectroscopy. American Mineralogist 92, 44–56.

Wood, B.J., Walter, M.J., and Wade, J. (2006) Accretion of the Earth and segregation of its core. Nature 441. 825–833.

Table 1. The pre-edge peak intensity of V, calculated log fO_2 relative to IW buffer, and averaged valence of Fe of measured μ-XANES spots.

	V intensity	IW	Fe valence
Inclusion glass			
Inc 1 spot 1	125	0.12±0.17	1.97±0.10
Inc 1 spot 2	112	0.00±0.17	1.89±0.10
Inc 2 spot 1	92	–0.18±0.17	1.95±0.10
Inc 2 spot 2	86	–0.23±0.17	1.95±0.10
Groundmass glass			
GM 1 spot 1	187	0.67±0.17	2.20±0.10
GM 2 spot 1	209	0.87±0.17	2.17±0.10
GM 2 spot 2	178	0.58±0.17	2.01±0.10
GM 3 spot 1	257	1.29±0.17	2.09±0.10
GM 3 spot 2	245	1.19±0.17	2.17±0.10
GM 3 spot 3	252	1.25±0.17	2.36±0.10
GM 4 spot 1	287	0.66±0.17	2.08±0.10
GM 4 spot 2	217	0.94±0.17	2.14±0.10
Synthesized glass			
IW±0	100	–0.10 [a)]	
IW+0.7	209	+0.87 [a)]	
IW+2.2	349	+2.11 [a)]	
Chromite	97		

[a)] Calculated from the calibration curve.

Figure Captions

Fig. 1. Photomicrograph (plane-polarized light) of Y98 thin section used in this study. Olivine megacrysts and pyroxenes dominate the groundmass. Dark materials are glassy mesostasis containing dendritic olivines and pyroxenes. Boxes identify XRF mapping areas shown in Figs. 3(A)–(C) and (I).

Fig. 2. The relationship between pre-edge peak intensity and oxygen fugacity for the synthetic glasses. The dashed line shows regression line used as a calibration curve for Y98.

Fig. 3. Back-scattered electron (BSE) and tricolor XRF mapping (Fe: red; Cr: green; Ca: blue) images. (D) Inc 1, (E) GM 1, (F) GM 2, (G) Inc 2, (H) GM 3, and (I) GM 4. White crosses shown in (D)–(I) denote the μ-XANES analytical spots.

Fig. 4. The V K-edge XANES spectra of (A) reference materials including three synthesized glasses, (B) and (C) μ-XANES analytical spots.

Fig. 5. Relationship between log fO_2 relative to IW and averaged oxidation states Fe.

Fig. 6. Simulation of irradiation effect on the log fO_2 relative to IW. Solid lines denote inclusion glasses with V content of 112 ppm crystallized at IW–0.23 and +0.12, whereas dashed lines represent groundmass glasses in which V concentration is assumed to be 93 ppm crystallized at IW+0.58 (measured lowest value), IW+1.29 (measured highest value), and IW0.93 (averaged value of groundmass).

Fig. 7. Summary of the relationship between isotopic ratio (ε^{143}Nd) and oxygen fugacity of martian meteorite. Open symbols represent later stage. The isotopic data of all the meteorites were obtained from Jones (2015), whereas oxygen fugacity of ALH A77005, Dhofar 019, EET-A, and SaU 005 were taken from Goodrich et al. (2003); EET-B, Los

Angeles, QUE 94201, Shergotty, and Zagami were cited from Herd et al. (2001). The oxygen fugacity of Dag 476, LAR 06319, NWA1968, and Tissint were reported by Herd et al. (2002), Peslier et al. (2010), and Herd (2006), and Castle and Herd (2017), respectively.

DOI: https://doi.org/10.2138/am-2020-7321

Figure 1

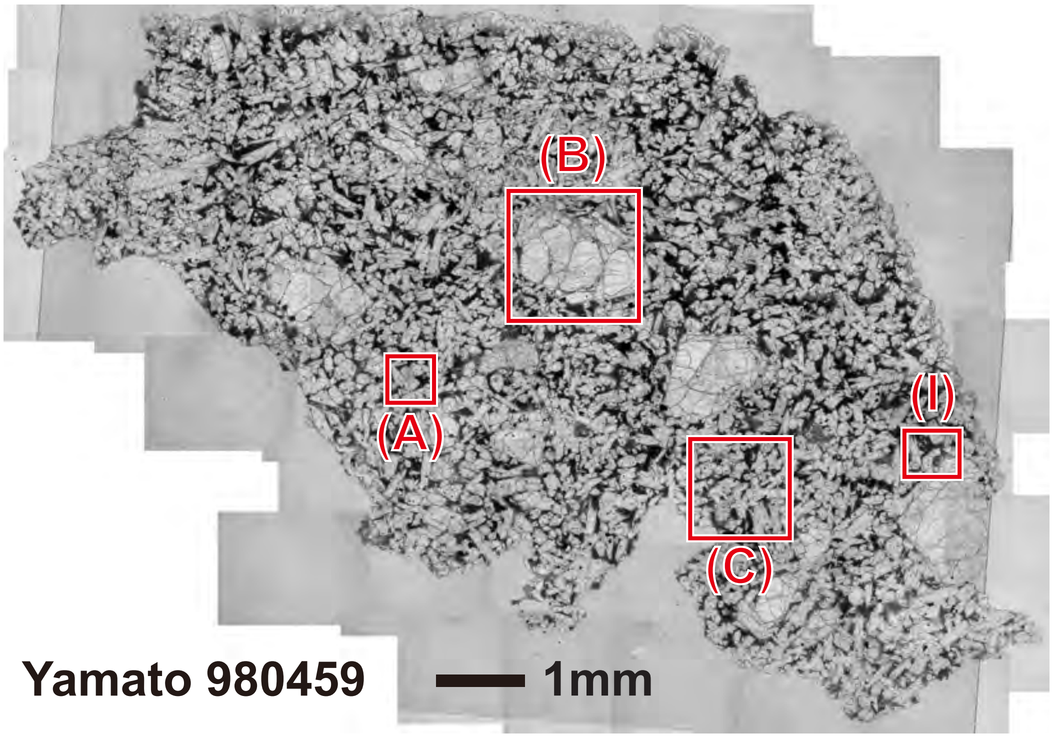

Figure 2

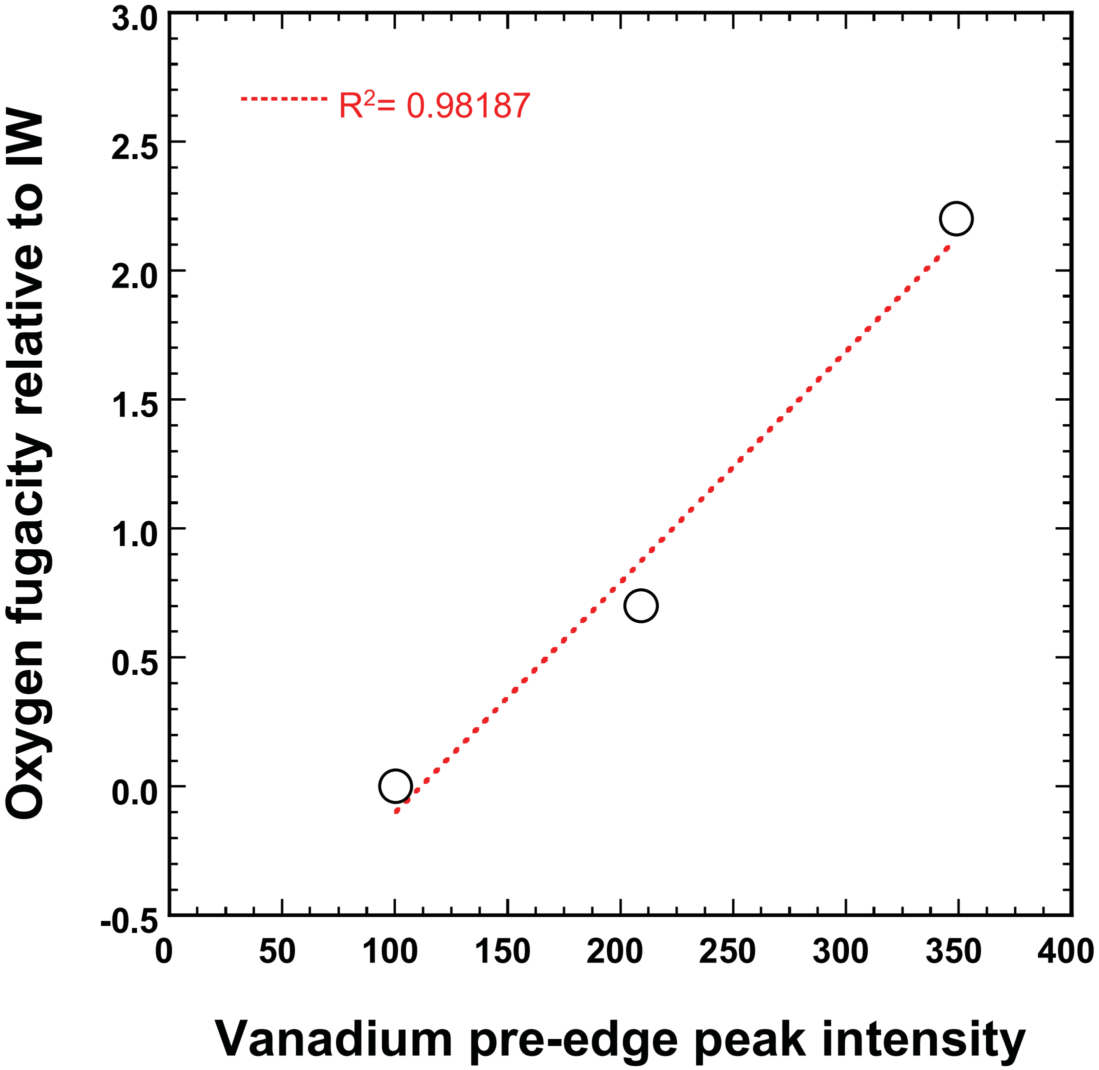
R^2= 0.98187
Oxygen fugacity relative to IW
3.0
2.5
2.0
1.5
1.0
0.5
0.0
-0.5
0
50
100
150
200
250
300
350
400
Vanadium pre-edge peak intensity

Figure 3

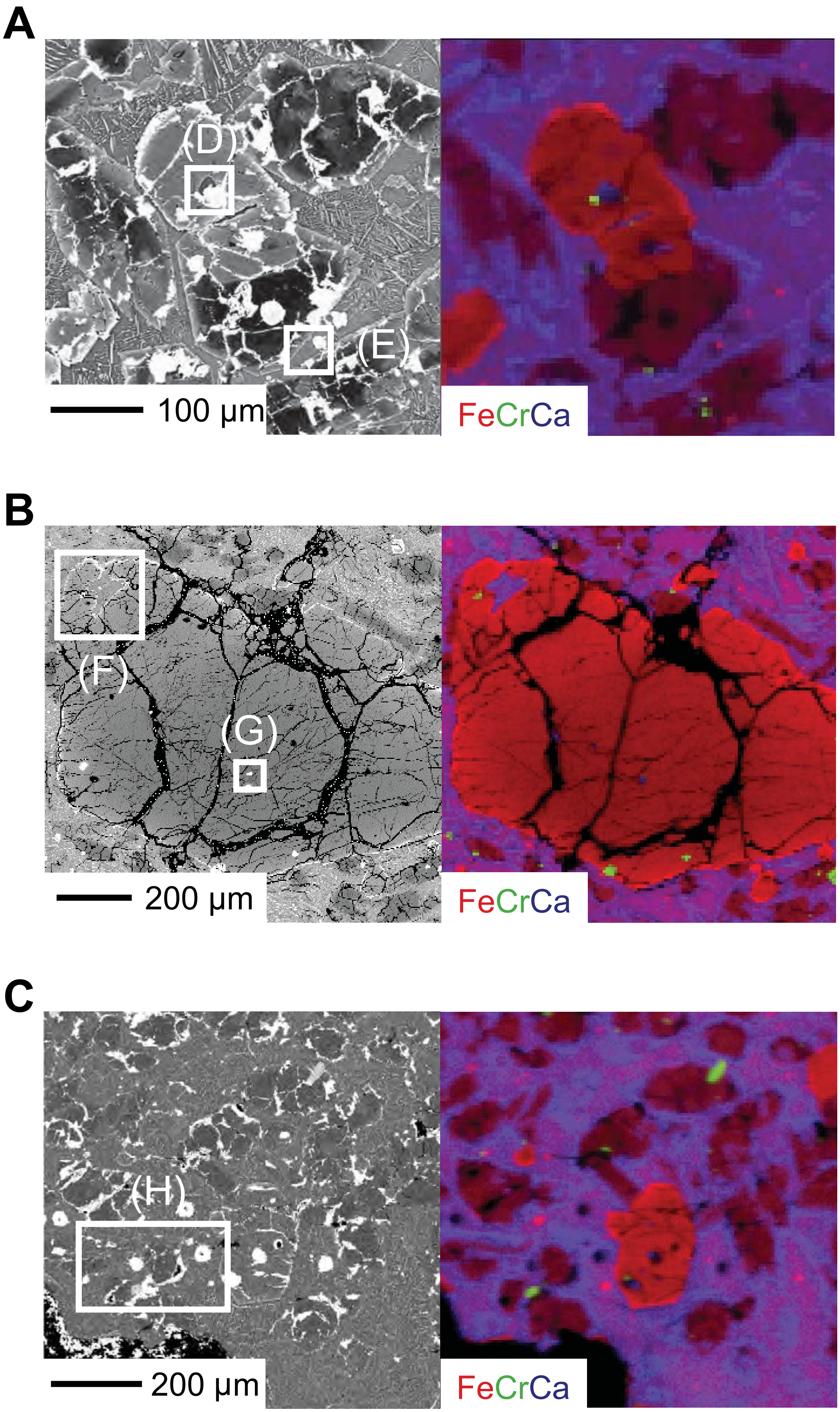

Figure 3

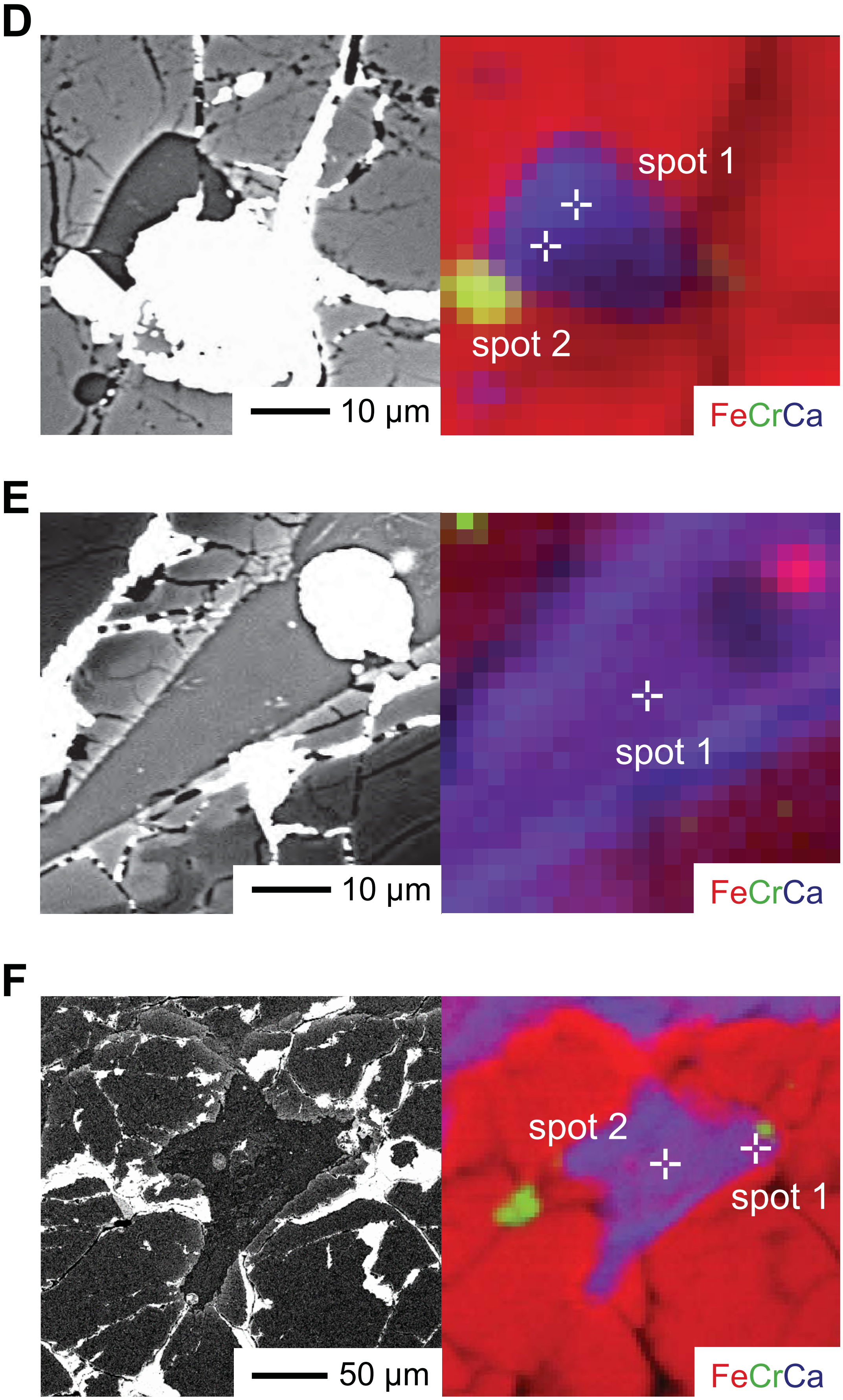
D
spot 1
spot 2
10 μm
FeCrCa
E
spot 1
10 μm
FeCrCa
F
spot 2
spot 1
50 μm
FeCrCa

DOI: https://doi.org/10.2138/am-2020-7321

Figure 3

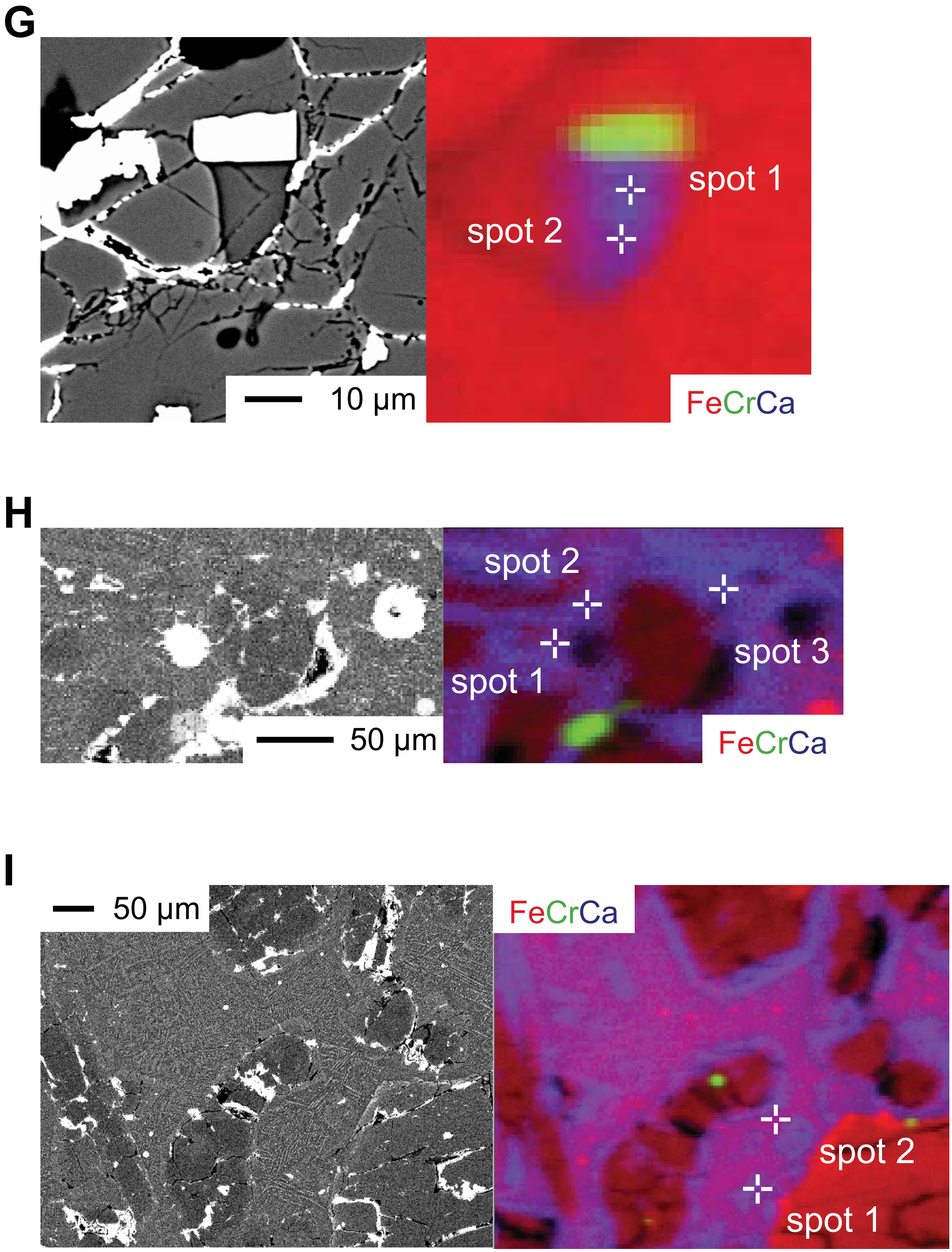

Figure 4

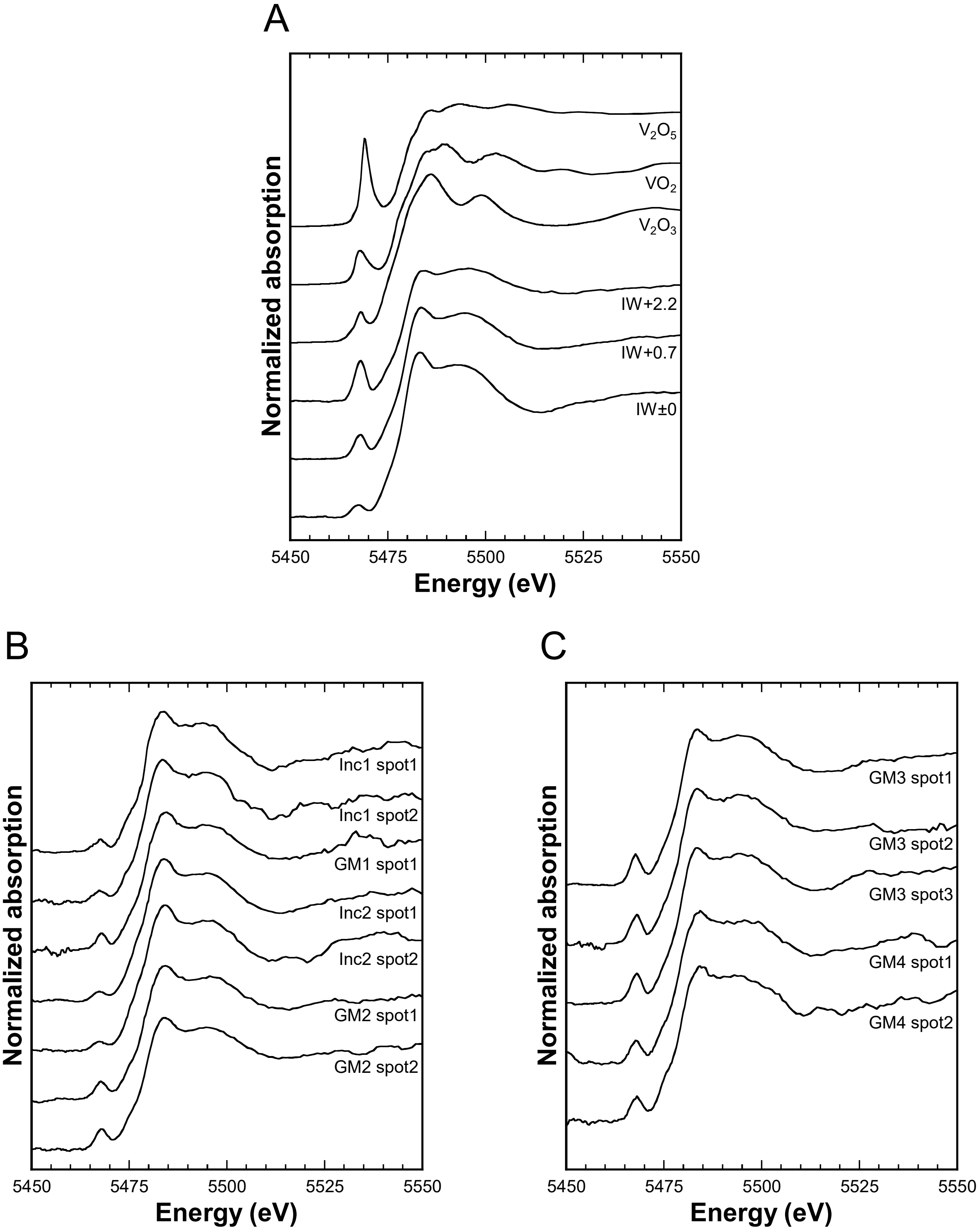
A
Normalized absorption
Energy (eV)
5450
5475
5500
5525
5550
V_2O_5
VO_2
V_2O_3
IW+2.2
IW+0.7
IW±0
B
Normalized absorption
Energy (eV)
Inc1 spot1
Inc1 spot2
GM1 spot1
Inc2 spot1
Inc2 spot2
GM2 spot1
GM2 spot2
C
Normalized absorption
Energy (eV)
GM3 spot1
GM3 spot2
GM3 spot3
GM4 spot1
GM4 spot2

Figure 5

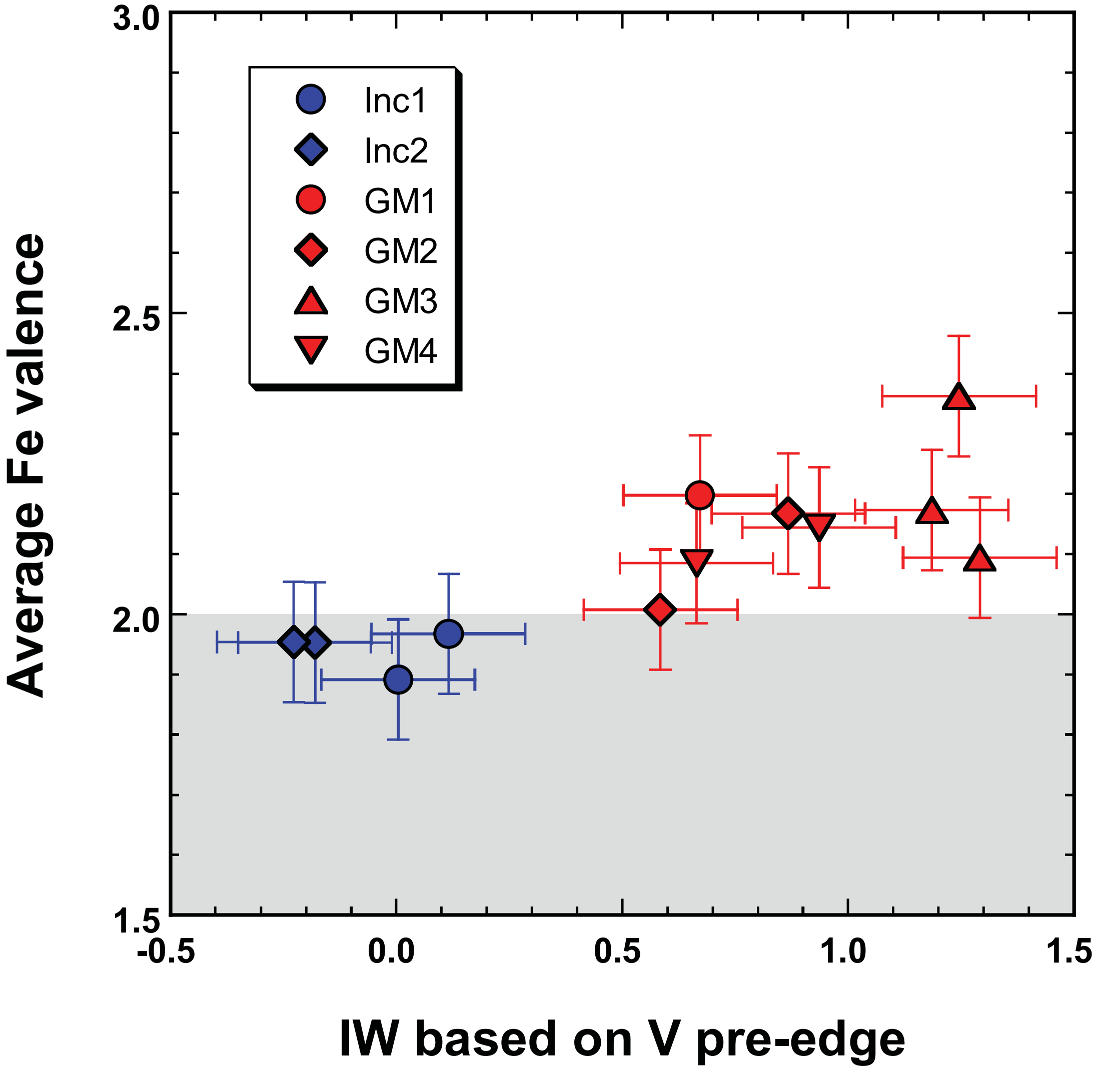
3.0
2.5
2.0
1.5
-0.5
0.0
0.5
1.0
1.5
Average Fe valence
IW based on V pre-edge
Inc1
Inc2
GM1
GM2
GM3
GM4

Figure 6

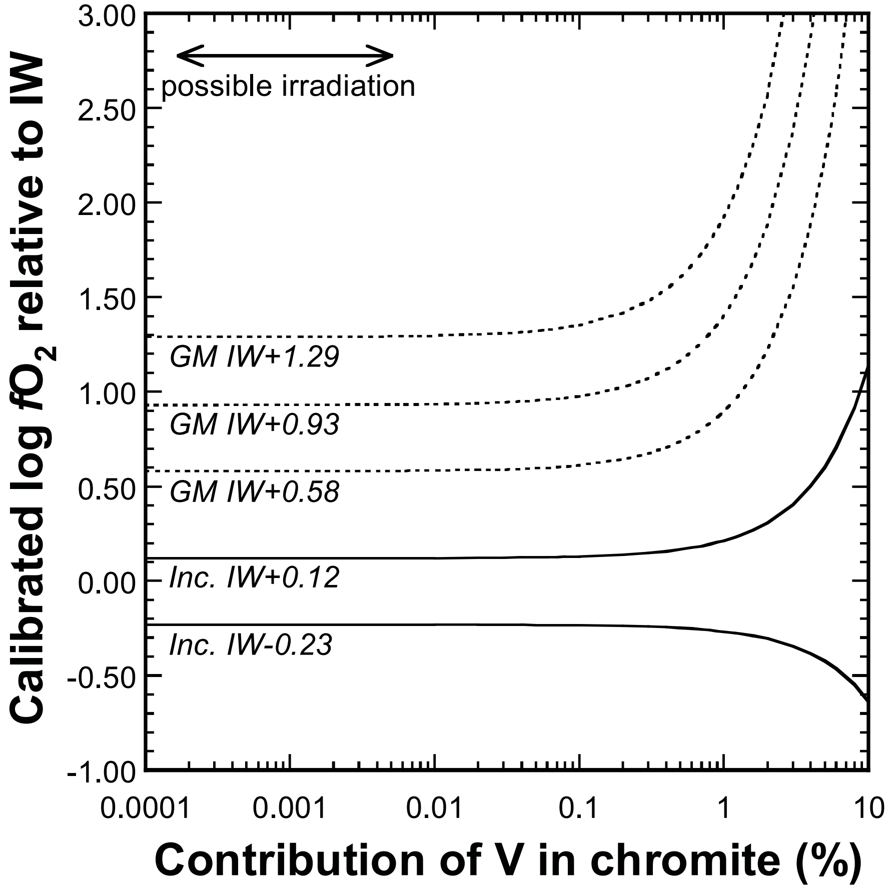
3.00
2.50
2.00
1.50
1.00
0.50
0.00
-0.50
-1.00
possible irradiation
GM IW+1.29
GM IW+0.93
GM IW+0.58
Inc. IW+0.12
Inc. IW-0.23
0.0001
0.001
0.01
0.1
1
10
Calibrated log fO_2 relative to IW
Contribution of V in chromite (%)

Figure 7

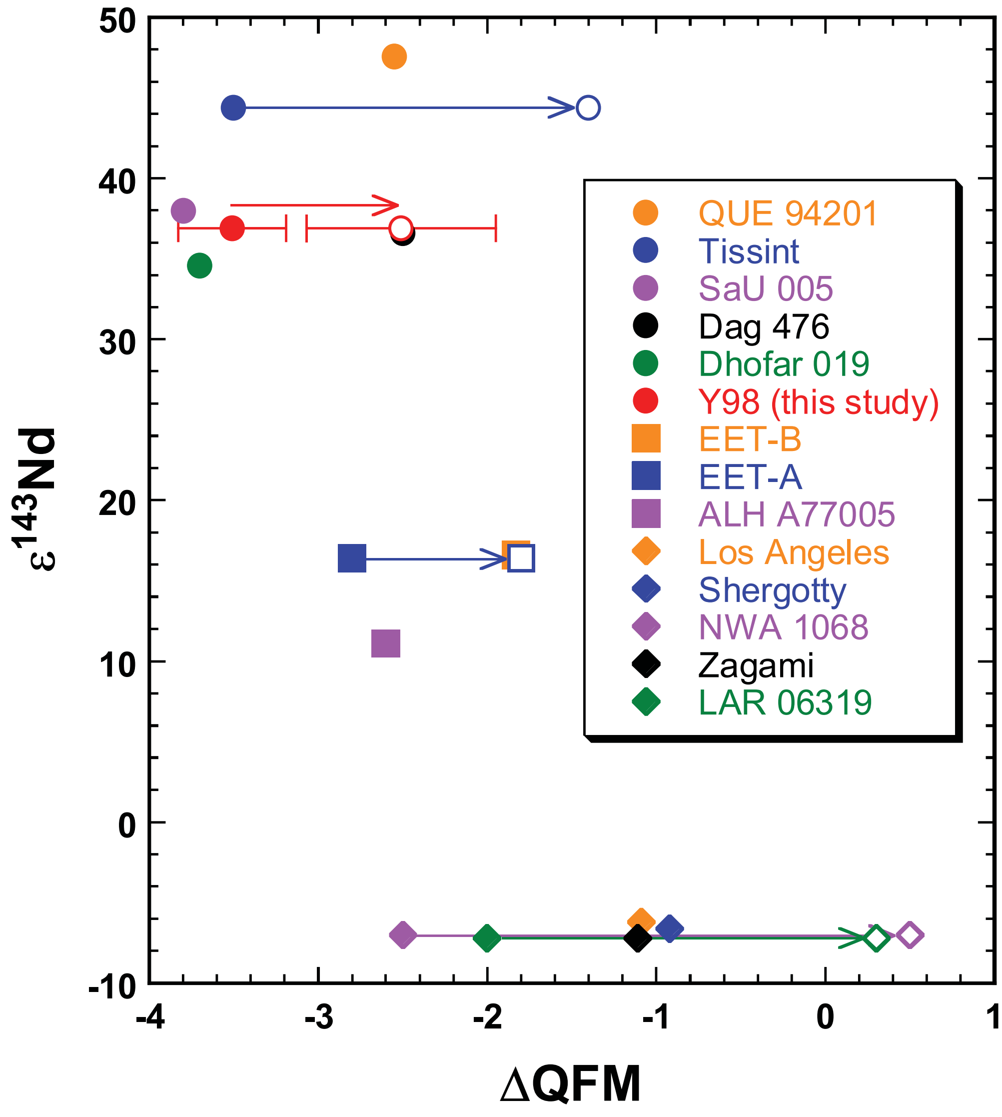
50
40
30
20
10
0
-10
-4
-3
-2
-1
0
1
ε143Nd
ΔQFM
● QUE 94201
● Tissint
● SaU 005
● Dag 476
● Dhofar 019
● Y98 (this study)
■ EET-B
■ EET-A
■ ALH A77005
◆ Los Angeles
◆ Shergotty
◆ NWA 1068
◆ Zagami
◆ LAR 06319